Check for updates

A biodegradable and rechargeable fiber battery†

Tenglong Mei, Chuang Wang, Meng Liao, Jiaxin Li, Liyuan Wang, Chengqiang Tang, Xuemei Sun, [iD] Bingjie Wang and Huisheng Peng [iD] *

It is critical to realize biodegradable and rechargeable batteries that are also flexible and safe for power supplies *in vivo*, yet they remain unavailable. Here, we discovered such a biocompatible battery by designing biodegradable fiber conductors incorporated with polydopamine/polypyrrole composite material as the anode and MnO_2 as the cathode, biodegradable chitosan as the separator and body fluid as the electrolyte. It can be directly injected into the body mini-invasively and well integrate with biological tissues without inducing immune responses. It delivered a specific capacity of 25.6 mA h g^{-1} with a retention of 69.1% after 200 charge/discharge cycles to power various biomedical devices. For instance, it was demonstrated to effectively power biosensors in the body. After completing the mission, it could be biodegraded, eliminating the need of surgery to remove it.

As a burgeoning technology, biodegradable electronics are promising in the field of disease diagnosis and treatment such as wound healing, disease tracking, drug delivery and tissue regeneration.[1–4] Different from traditional chronic medical implants, they can entirely or partially biodegrade in the body after completing their mission, eliminating the need of second surgery for device retrieval and potential chronic inflammatory responses.[5–14] Among them, biodegradable power supply such as a battery is obviously an indispensable part. However, it remains challenging to realize such batteries due to the simultaneous high demand for miniaturization, flexibility and safety.[15–19] Current biodegradable batteries are bulky and rigid typically due to the use of metal sheets (Mg, Zn, Fe, W, and Mo) as electrodes.[5,20–25] Hard metal electrodes and side reactions[20,21,26] (*e.g.*, corrosion and dissolution) damage surrounding tissues.

State Key Laboratory of Molecular Engineering of Polymers, Department of Macromolecular Science, Laboratory of Advanced Materials, Fudan University, Shanghai 200438, China. E-mail: penghs@fudan.edu.cn

† Electronic supplementary information (ESI) available. See DOI: 10.1039/d1ta01507a

Here, we realized a biodegradable and rechargeable aqueous fiber battery by designing biodegradable fiber electrodes and a chitosan separator with body fluid as electrolyte (Fig. 1). Benefiting from the one-dimensional configuration and high flexibility, the fiber battery could be directly injected into the body with minimal invasion. It showed decent power capability and was demonstrated to successfully power a biosensor that detected pressure changes *in vivo*. After the use, it was biodegraded and the entire biodegradation process proved nontoxic and non-interfering with the body.

The fiber power system was made from an aqueous sodium-ion battery by a facile and environmentally friendly process (Fig. 2a). As an essential component, conducting fiber was first prepared by sputtering a thin layer of gold (~80 nm) onto a polyglycolic acid yarn (Fig. S1 and S2†), followed by twisting it into a bundle. Here, 10 yarns were used to fabricate a conducting fiber (Fig. S3†). The conducting fiber was then incorporated
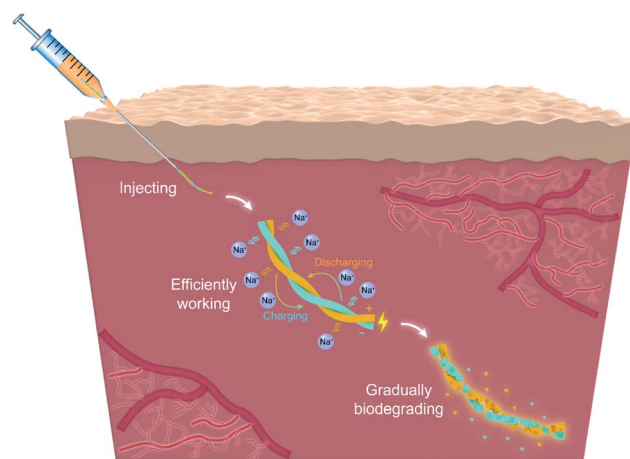

Fig. 1 Schematic illustration of the implantation process by direct injection without surgery, working process and biodegradation after the use in the body.

10104 | *J. Mater. Chem. A*, 2021, **9**, 10104–10109

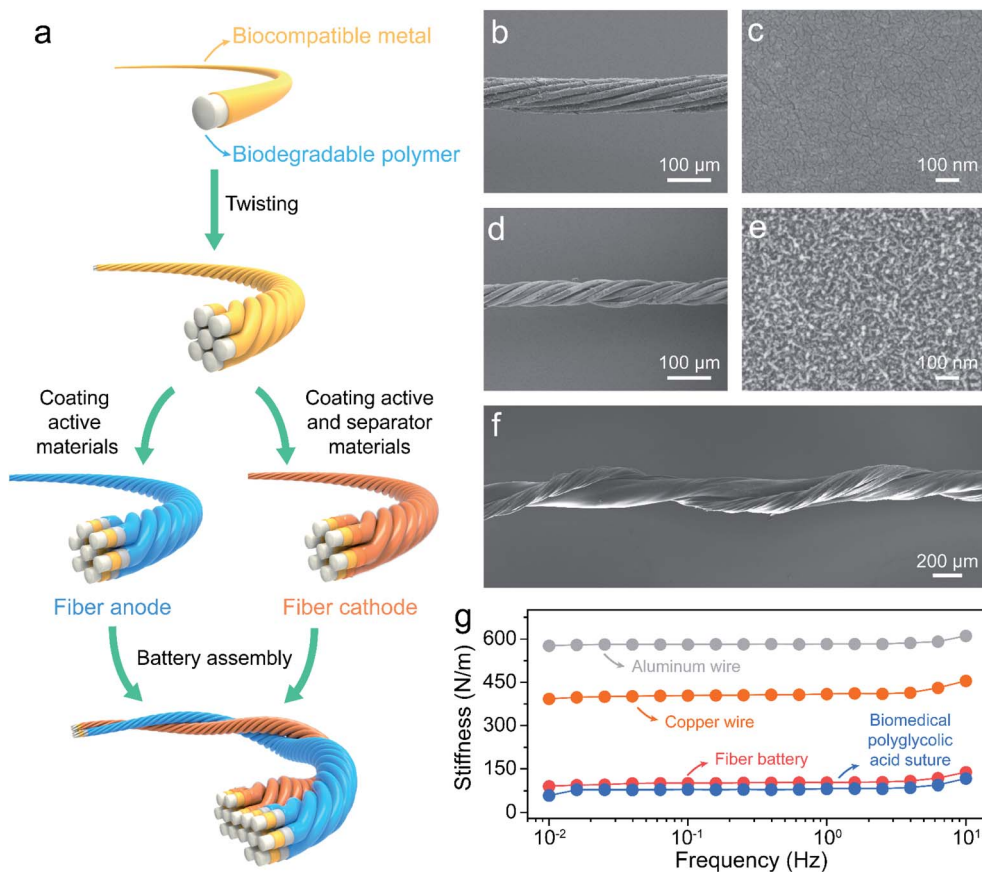This journal is © The Royal Society of Chemistry 2021

Fig. 2 Fabrication, structure and mechanical properties of the fiber battery. (a) Schematic diagram of the fabrication process. (b and c) Scanning electron microscopy images of the fiber anode at low and high magnification, respectively. (d and e) Scanning electron microscopy images of the fiber cathode at low and high magnification, respectively. (f) Scanning electron microscopy image of an assembled fiber battery. (g) Stiffness comparison of the fiber battery with traditional metal wires and biomedical polyglycolic acid suture.

with polydopamine/polypyrrole and MnO_2 as the anode and cathode, respectively. Both fiber electrodes were approximately 70 μm in diameter (Fig. 2b and d), and the active materials were uniformly and compactly attached on the surface of the conducting fiber (Fig. 2c and e). To prevent short circuits, biodegradable chitosan was used as the separator with decent ionic conductivity and controllable thickness (Fig. S4 and S5, Table S1†). Here, the fiber cathode was dip-coated with a layer of chitosan with a thickness of approximately 10 μm (Fig. S6†). A multi-layered coaxial structure was shared by the fiber anode and cathode (Fig. S7†).

The anode and cathode were finally twisted together to produce the fiber battery (Fig. 2f) which was flexible and robust (Fig. S8†). Its stiffness was measured using a dynamic mechanical analyzer in single-cantilever mode. In the frequency range of 0.01–10 Hz, the fiber battery demonstrated stable stiffness with values of 90–138 N m^{-1}, much lower than those of traditional fiber collectors such as aluminum (577–611 N m^{-1}) and copper (392–455 N m^{-1}) wires and comparable to that of a biomedical polyglycolic acid suture (60–117 N m^{-1}) (Fig. 2g). In other words, it showed high flexibility and would not damage soft biological tissues during use.

Electrochemical properties were first investigated *in vitro*. To simulate the humoral environment, 1× phosphate-buffered saline was used as the electrolyte. Both fiber electrodes could charge and discharge stably, and they showed good rate capability and high cycling stability (Fig. S9 and S10†). The resulting fiber battery demonstrated a specific capacity of 24.4 mA h g^{-1} at a current density of 1000 mA g^{-1} (Fig. 3a and b) with high stability upon cycling (Fig. S11†). After 1000 cycles of bending at a bending angle of 180°, the capacity was maintained as 89.1% (Fig. S12†). The fiber battery was then immersed in 1× phosphate-buffered saline at 37 °C for degradation evaluation. During the first two weeks, the fiber battery was intact and might work since polyglycolic acid remained relatively stable (Fig. 3c), and the specific capacity decreased with time (Fig. 3d). Then due to the intensified hydrolysis of polyglycolic acid, the fiber battery started to degrade into scattered fragments and failed to work, and it was almost fully degraded at the end of twelve weeks (Fig. 3c and S13†). Note that the degradation velocity and the stable operation interval can be controlled by the rational design and optimization of biodegradable polymers.

Biocompatibility was also systematically investigated to ensure high safety *in vivo*. Representative haematoxylin and
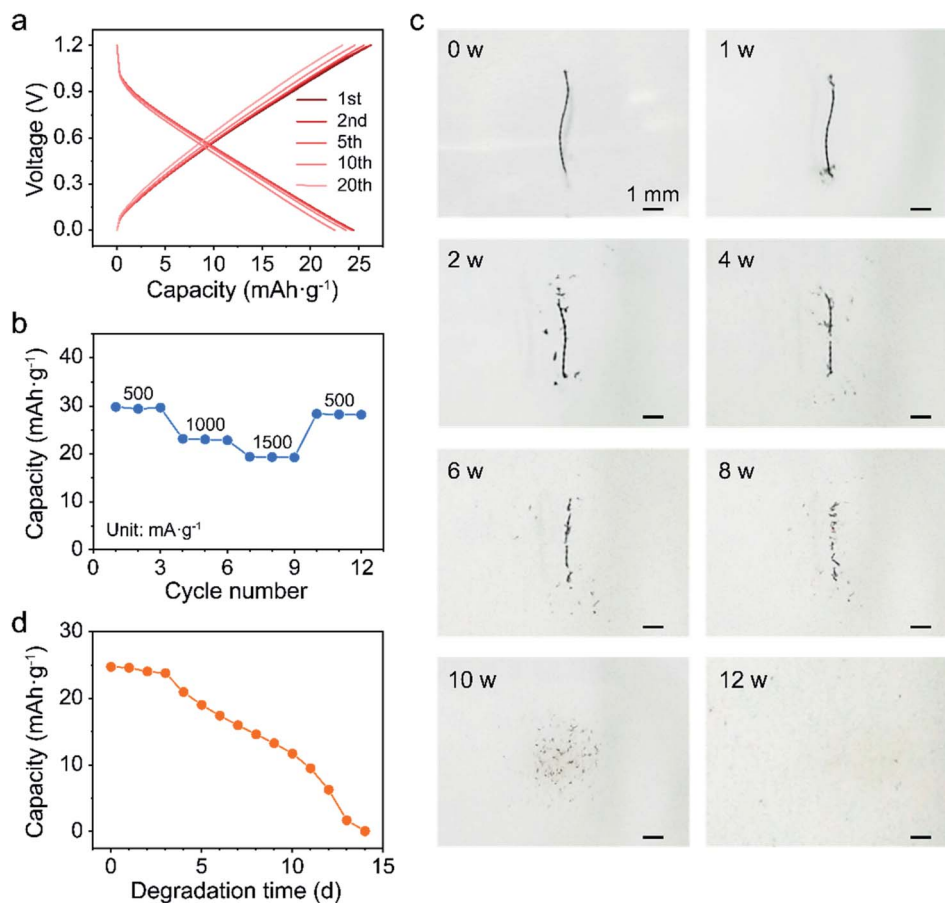
Fig. 3 Electrochemical and degradation properties of the fiber battery *in vitro*. (a) Galvanostatic charge and discharge profiles at a current density of 1000 mA g^{-1}. (b) Rate capability at increasing current densities from 500 to 1500 mA g^{-1}. (c) Degradation in 1× phosphate-buffered saline at 37 °C. (d) Evolution of specific capacity upon increasing degradation time at a current density of 1000 mA g^{-1}.

eosin (H&E) staining showed that the tissue morphology around the fiber batteries at different states of charge demonstrated no obvious differences compared with the control group (without implants) after four weeks (Fig. 4a, b, S14c and d†), indicating high integration between the fiber batteries and the tissue.[27] F4/80 and LY-6G immunofluorescence staining were also performed to study whether there existed immune responses. The immunofluorescence signals around the fiber batteries at different states of charge were similar to those of the control group after four weeks (Fig. 4c–f and S14e–h†). No obvious macrophage aggregation and inflammatory response were observed around the fiber batteries, suggesting their superior biocompatibility. Moreover, the fiber batteries at different states of charge demonstrated negligible toxicity and side effects as revealed by the H&E staining of main organs such as the heart, liver, spleen, lung and kidney, and almost no differences were found in comparison to the control group after four weeks (Fig. S15†).

In addition, to determine the effects of biodegradation on the organism, the H&E staining of the subcutaneous tissues at implantation sites and main organs was analyzed further after the fiber batteries at different states of charge completely biodegraded *in vivo*. The tissue morphology

demonstrated no abnormalities (Fig. S16†) and the main organs in the experimental group showed no obvious pathological changes or tissue damage when compared with the control group (Fig. 4g and S17†), so the biodegradation of the fiber batteries induced no obvious damage to the body. The nontoxicity of the fiber battery in the whole life cycle was derived from the intrinsic nature of all its components. Polyglycolic acid, polydopamine and chitosan finally biodegraded into harmless substances; gold was safe *in vivo* owing to its inert nature;[28] polypyrrole demonstrated good biocompatibility and is widely used in the biomedical field;[29–32] MnO$_2$ has a considerable recommended daily allowance without interfering with the body.[33]

Benefiting from the one-dimensional configuration and high flexibility, the fiber battery was directly injected into the body. The resulting wound was only about 300 μm in size (Fig. S18†). Owing to the rational design, both conducting fiber substrates could be extracted out of the body (Fig. 5a and b). Therefore, the fiber battery could be easily recharged *via* an external power source if necessary after energy depletion. After injection into the abdominal subcutis of an experimental mouse, it demonstrated a specific capacity of 25.6 mA h g^{-1} at a current density of 1000 mA g^{-1} in the
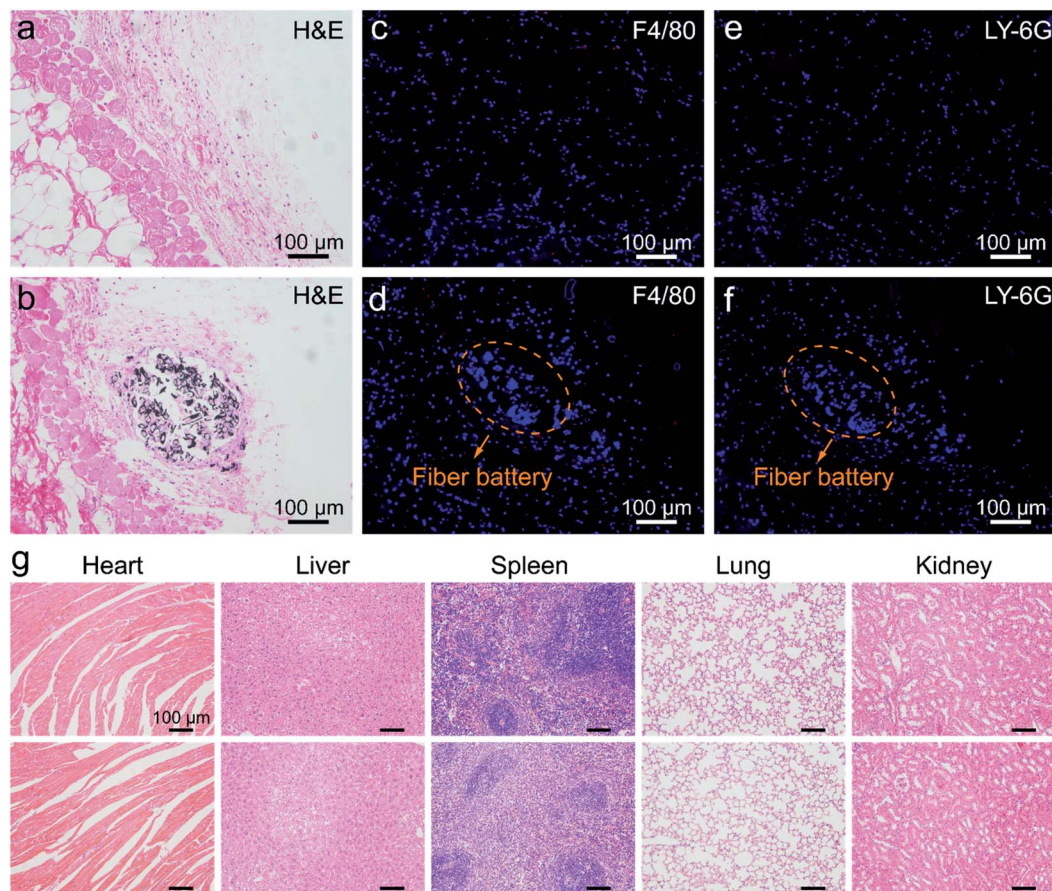
Fig. 4 Biocompatibility of the fiber battery. (a and b) Representative H&E sections of subcutaneous tissues without and with implantation of the fiber battery (at a voltage of 1.2 V) after 4 weeks, respectively. (c and d) F4/80-labelled sections of subcutaneous tissues without and with implantation of the fiber battery (at a voltage of 1.2 V) after 4 weeks, respectively. The nucleus is shown in blue (DAPI) while F4/80 is shown in red. The orange dotted ellipse indicates the position of the fiber battery. (e and f) LY-6G-labelled sections of subcutaneous tissues without and with implantation of the fiber battery (at a voltage of 1.2 V) after 4 weeks, respectively. The nucleus is shown in blue (DAPI) while LY-6G is shown in red. The orange dotted ellipse indicates the position of the fiber battery. (g) Representative H&E sections obtained from major organs including the heart, liver, spleen, lung, and kidney of mice. Top row: control group (without implantation of the fiber battery). Bottom row: experimental group (after the implanted fiber battery at a voltage of 1.2 V had completely biodegraded *in vivo*).

voltage window of 0–1.2 V (Fig. 5c) without short circuits (Fig. S19†). The fiber battery also showed good rate capability with specific capacities of 28.7 mA h g^{-1} and 20.6 mA h g^{-1} at 500 and 1500 mA g^{-1}, respectively (Fig. 5d). The capacity dropped only marginally at higher rates and immediately recovered with the reversal of the current density. After 200 charge/discharge cycles at 1000 mA g^{-1}, the fiber battery still demonstrated a specific capacity of 17.7 mA h g^{-1} with a retention of 69.1% (Fig. 5e). The high flexibility of the fiber battery also laid a solid foundation for stable operation against varying deformations including pressing, bending and stretching *in vivo* (Fig. 5f).

As a demonstration of its application, the fiber battery was then used to power a fiber sensor that detects pressure changes in the implanted area (Fig. 6a and b). After completing the required power supply, the fiber battery biodegraded as designed. Polyglycolic acid, polydopamine and chitosan fully biodegraded upon hydrolysis and enzymolysis.[34,35] Gold, polypyrrole and MnO$_2$ were eventually eliminated by renal excretion, phagocytosis and/or endocytosis after biodegradation into fragments of several hundred nanometers.[22,36–38] In fact, the fiber battery completely disappeared after ten weeks eliminating the need of surgical removal and the specific capacity decreased with the biodegradation time (Fig. 6c and d).

In summary, a biodegradable and rechargeable fiber battery was realized for the first time by rationally designing materials and architecture. It showed unique advantages of small size, high flexibility and rechargeability (Table S2†). Specifically, it could be directly injected into the body in a minimally invasive way and it integrated stably with soft biological tissues without damaging them. The fiber battery demonstrated high electrochemical properties to effectively power biomedical devices and could then be safely biodegraded without the need of surgical removal after completing the mission *in vivo*. This work provides a general and effective paradigm for the development of next-generation biodegradable batteries.
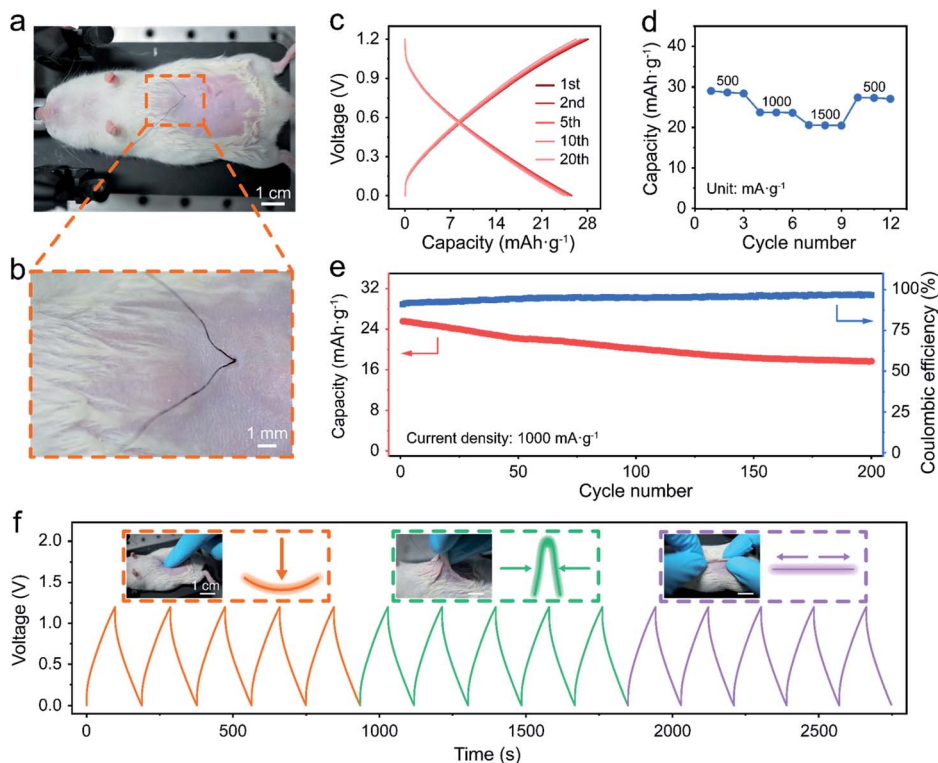
This journal is © The Royal Society of Chemistry 2021

J. Mater. Chem. A, 2021, **9**, 10104–10109 | **10107**

Fig. 5 Electrochemical properties of the fiber battery *in vivo*. (a and b) Photographs of a mouse injected with the fiber battery at low and high magnification, respectively. (c) Galvanostatic charge and discharge profiles at a current density of 1000 mA g^{-1}. (d) Rate capability at increasing current densities from 500 to 1500 mA g^{-1}. (e) Cycling performance at a current density of 1000 mA g^{-1}. (f) Galvanostatic charge and discharge profiles of the fiber battery upon pressing, bending and stretching at a current density of 1000 mA g^{-1}.
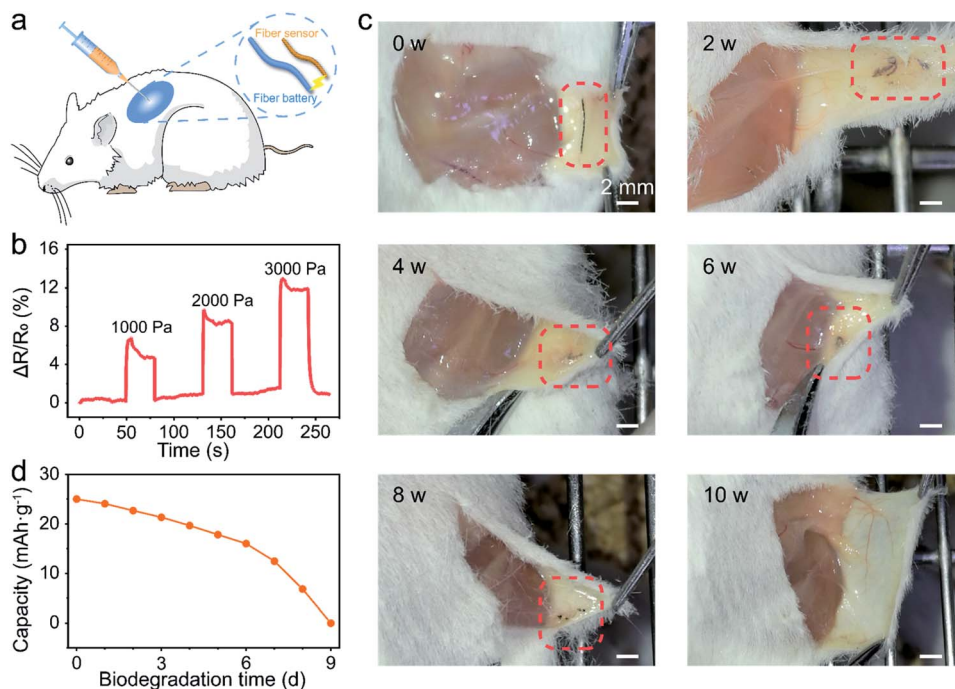

Fig. 6 Application demonstration and biodegradation characterization of the fiber battery *in vivo*. (a) Schematic illustration of the fiber battery powering a fiber pressure sensor *in vivo*. (b) Response of the fiber sensor to pressure changes in the implanted area. (c) Photographs showing the biodegradation process of the fiber battery with time. It disappeared after 10 weeks. (d) Evolution of specific capacity upon increasing biodegradation time at a current density of 1000 mA g^{-1}.

10108 | *J. Mater. Chem. A*, 2021, **9**, 10104–10109

This journal is © The Royal Society of Chemistry 2021

Conflicts of interest

There are no conflicts to declare.

Acknowledgements

References

1 L. Xu, S. R. Gutbrod, A. P. Bonifas, Y. Su, M. S. Sulkin, N. Lu, H. J. Chung, K. I. Jang, Z. Liu, M. Ying, C. Lu, R. C. Webb, J. S. Kim, J. I. Laughner, H. Cheng, Y. Liu, A. Ameen, J. W. Jeong, G. T. Kim, Y. Huang, I. R. Efimov and J. A. Rogers, *Nat. Commun.*, 2014, **5**, 3329–3338.

2 S. K. Kang, R. K. J. Murphy, S. W. Hwang, S. M. Lee, D. V. Harburg, N. A. Krueger, J. Shin, P. Gamble, H. Cheng, S. Yu, Z. Liu, J. G. McCall, M. Stephen, H. Ying, J. Kim, G. Park, R. C. Webb, C. H. Lee, S. Chung, D. S. Wie, A. D. Gujar, B. Vemulapalli, A. H. Kim, K. M. Lee, J. Cheng, Y. Huang, S. H. Lee, P. V. Braun, W. Z. Ray and J. A. Rogers, *Nature*, 2016, **530**, 71–76.

3 K. J. Yu, D. Kuzum, S. W. Hwang, B. H. Kim, H. Juul, N. H. Kim, S. M. Won, K. Chiang, M. Trumpis, A. G. Richardson, H. Cheng, H. Fang, M. Thompson, H. Bink, D. Talos, K. J. Seo, H. N. Lee, S. K. Kang, J. H. Kim, J. Y. Lee, Y. Huang, F. E. Jensen, M. A. Dichter, T. H. Lucas, J. Viventi, B. Litt and J. A. Rogers, *Nat. Mater.*, 2016, **15**, 782–791.

4 H. Tao, S. W. Hwang, B. Marelli, B. An, J. E. Moreau, M. Yang, M. A. Brenckle, S. Kim, D. L. Kaplan, J. A. Rogers and F. G. Omenetto, *Proc. Natl. Acad. Sci. U. S. A.*, 2014, **111**, 17385–17389.

5 M. Tsang, A. Armutlulu, A. W. Martinez, S. A. B. Allen and M. G. Allen, *Microsyst. Nanoeng.*, 2015, **1**, 15024.

6 S. W. Hwang, H. Tao, D. H. Kim, H. Cheng, J. K. Song, E. Rill, M. A. Brenckle, B. Panilaitis, S. M. Won, Y. S. Kim, Y. M. Song, K. J. Yu, A. Ameen, R. Li, Y. Su, M. Yang, D. L. Kaplan, M. R. Zakin, M. J. Slepian, Y. Huang, F. G. Omenetto and J. A. Rogers, *Science*, 2012, **337**, 1640–1644.

7 C. R. Gordijo, A. J. Shuhendler and X. Y. Wu, *Adv. Funct. Mater.*, 2010, **20**, 1404–1412.

8 M. Irimia-Vladu, *Chem. Soc. Rev.*, 2014, **43**, 588–610.

9 A. Sokolov, B. C. Hellerud, E. A. Johannessen and T. E. Mollnes, *J. Biomed. Mater. Res., Part A*, 2012, **100**, 1142–1150.

10 S. W. Hwang, G. Park, H. Cheng, J. K. Song, S. K. Kang, L. Yin, J. H. Kim, F. G. Omenetto, Y. Huang, K. M. Lee and J. A. Rogers, *Adv. Mater.*, 2014, **26**, 1992–2000.

11 C. J. Bettinger and Z. Bao, *Adv. Mater.*, 2010, **22**, 651–655.

12 R. Li, L. Wang, D. Kong and L. Yin, *Bioact. Mater.*, 2018, **3**, 322–333.

13 H. Acar, S. Çinar, M. Thunga, M. R. Kessler, N. Hashemi and R. Montazami, *Adv. Funct. Mater.*, 2014, **24**, 4135–4143.

14 G. Lee, S. K. Kang, S. M. Won, P. Gutruf, Y. R. Jeong, J. Koo, S. S. Lee, J. A. Rogers and J. S. Ha, *Adv. Energy Mater.*, 2017, **7**, 1–12.

15 W. A. Haider, M. Tahir, L. He, H. A. Mirza, R. Zhu, Y. Han and L. Mai, *ACS Cent. Sci.*, 2020, **6**, 1901–1915.

16 X. Jia, Y. Yang, C. Wang, C. Zhao, R. Vijayaraghavan, D. R. Macfarlane, M. Forsyth and G. G. Wallace, *ACS Appl. Mater. Interfaces*, 2014, **6**, 21110–21117.

17 X. Hu, Z. Li and J. Chen, *Angew. Chem., Int. Ed.*, 2017, **56**, 5785–5789.

18 X. Wang, J. Gao, Z. Cheng, N. Chen and L. Qu, *Angew. Chem., Int. Ed.*, 2016, **55**, 14643–14647.

19 H. Tian, J. Qin, D. Hou, Q. Li, C. Li, Z. S. Wu and Y. Mai, *Angew. Chem., Int. Ed.*, 2019, **131**, 10279–10284.

20 X. Huang, D. Wang, Z. Yuan, W. Xie, Y. Wu, R. Li, Y. Zhao, D. Luo, L. Cen, B. Chen, H. Wu, H. Xu, X. Sheng, M. Zhang, L. Zhao and L. Yin, *Small*, 2018, **14**, 1800994.

21 L. Yin, X. Huang, H. Xu, Y. Zhang, J. Lam, J. Cheng and J. A. Rogers, *Adv. Mater.*, 2014, **26**, 3879–3884.

22 X. Jia, C. Wang, V. Ranganathan, B. Napier, C. Yu, Y. Chao, M. Forsyth, F. G. Omenetto, D. R. Macfarlane and G. G. Wallace, *ACS Energy Lett.*, 2017, **2**, 831–836.

23 V. Edupuganti and R. Solanki, *J. Power Sources*, 2016, **336**, 447–454.

24 P. Nadeau, D. El-Damak, D. Glettig, Y. L. Kong, S. Mo, C. Cleveland, L. Booth, N. Roxhed, R. Langer, A. P. Chandrakasan and G. Traverso, *Nat. Biomed. Eng.*, 2017, **1**, 0022.

25 X. Jia, C. Wang, C. Zhao, Y. Ge and G. G. Wallace, *Adv. Funct. Mater.*, 2016, **26**, 1454–1462.

26 T. Zhang, Z. Tao and J. Chen, *Mater. Horizons*, 2014, **1**, 196–206.

27 L. Wang, S. Xie, Z. Wang, F. Liu, Y. Yang, C. Tang, X. Wu, P. Liu, Y. Li, H. Saiyin, S. Zheng, X. Sun, F. Xu, H. Yu and H. Peng, *Nat. Biomed. Eng.*, 2020, **4**, 159–171.

28 M. Longmire, P. L. Choyke and H. Kobayashi, *Nanomedicine*, 2008, **3**, 703–717.

29 S. Geetha, C. R. K. Rao, M. Vijayan and D. C. Trivedi, *Anal. Chim. Acta*, 2006, **568**, 119–125.

30 X. Wang, X. Gu, C. Yuan, S. Chen, P. Zhang, T. Zhang, J. Yao, F. Chen and G. Chen, *J. Biomed. Mater. Res., Part A*, 2004, **68**, 411–422.

31 A. Ramanaviciene and A. Ramanavicius, *Crit. Rev. Anal. Chem.*, 2002, **32**, 245–252.

32 P. M. George, A. W. Lyckman, D. A. Lavan, A. Hegde, Y. Leung, R. Avasare, C. Testa, P. M. Alexander, R. Langer and M. Sur, *Biomaterials*, 2005, **26**, 3511–3519.

33 *Toxicological Profile for Manganese*, ed. C. J. Portier, U.S. Department of Health and Human Services 7439-96-5, 2012.

34 T. Sun, Z. J. Li, H. G. Wang, D. Bao, F. L. Meng and X. B. Zhang, *Angew. Chem., Int. Ed.*, 2016, **55**, 10662–10666.

35 Y. Liu, K. Ai and L. Lu, *Chem. Rev.*, 2014, **114**, 5057–5115.

36 Y. S. Jeong, W. K. Oh, S. Kim and J. Jang, *Biomaterials*, 2011, **32**, 7217–7225.

37 S. Kim, W. K. Oh, Y. S. Jeong, J. Y. Hong, B. R. Cho, J. S. Hahn and J. Jang, *Biomaterials*, 2011, **32**, 2342–2350.

38 H. T. Nguyen, S. Sapp, C. Wei, J. K. Chow, A. Nguyen, J. Coursen, S. Luebben, E. Chang, R. Ross and C. E. Schmidt, *J. Biomed. Mater. Res., Part A*, 2014, **102**, 2554–2564.

This journal is © The Royal Society of Chemistry 2021

J. Mater. Chem. A, 2021, **9**, 10104–10109 | **10109**